EFDA–JET–PR(10)70

K.K. Kirov, Yu. Baranov, Th. Gerbaud, M. Goniche, J. Mailloux, M-L. Mayoral,
J. Ongena, S. Schmuck and JET EFDA contributors

Analysis of EC Emission by Fast Electrons Generated by LHCD at JET

Analysis of EC Emission by Fast Electrons Generated by LHCD at JET

K.K. Kirov[1], Yu. Baranov[1], Th. Gerbaud[1,2], M. Goniche[2], J. Mailloux[1], M-L. Mayoral[1], J. Ongena[3], S. Schmuck[1,4] and JET EFDA contributors*

JET-EFDA, Culham Science Centre, OX14 3DB, Abingdon, UK

[1]EURATOM-CCFE Fusion Association, Culham Science Centre, OX14 3DB, Abingdon, OXON, UK
[2]Association EURATOM-CEA, CEA/DSM/IRFM, Cadarache 13108 Saint Paul Lez Durance, France
[3]Plasmaphysics Laboratory, Association EURATOM-Belgian State, TEC partner Koninklijke Militaire School - Ecole Royale Militaire, B-1000 Brussels Belgium.
[4]Max-Planck-Institut für Plasmaphysik, Teilinsitut Greifswald, EURATOM-Assoziation, D-17491 Greifswald, Germany
** See annex of F. Romanelli et al, "Overview of JET Results", (23rd IAEA Fusion Energy Conference, Daejon, Republic of Korea (2010)).*

Preprint of Paper to be submitted for publication in
Plasma Physics and Controlled Fusion

ABSTRACT

Heating and driving non-inductive current in plasmas by means of Radio Frequency (RF) waves in the range of the Lower Hybrid (LH) frequencies is important for Steady State (SS) operation in fusion [1]. The penetration of LH waves at higher densities has been recently reviewed [2] in order to assess the Lower Hybrid Current Drive (LHCD) performance in conditions as close as possible to the ITER SS scenario. The analysis of various experiments performed on C-Mod, FTU, Tore Supra and JET indicate [2] a degradation of the Current Drive (CD) efficiency when the plasma density is increased, while at the same time the LH wave absorption shifts to the plasma periphery. JET pulses in H-mode confirm this trend and in addition it was found that the accessibility condition is not the main parameter to explain the reduction in the CD efficiency. This paper discusses further the LH deposition in H-mode plasmas and in particular it shows that lower pedestal density and higher temperature are beneficial regarding the LH wave penetration. The investigation presented here is based on the analysis of the Electron Cyclotron Emission (ECE) spectra in plasmas with fast electrons generated by LH waves. The study includes the numerical calculation of the ECE intensity and a comparison with experimental profiles in the plasma periphery for optically thin frequencies.

1. INTRODUCTION

LH waves are widely recognised as the most effective source of off-axis non-inductive current drive in fusion plasma [1], [3]. Their main applications nowadays include fully non-inductive operation and shaping the plasma current profile thus reducing the magnetic shear in order to avoid instabilities related to the peaked current in the plasma centre. The latter helps suppressing the turbulence-enhanced transport, which in turn is reduced significantly thus forming an Internal Transport Barrier (ITB) in the core [4], [5]. Based on these unique features LH is under consideration as a current drive system on ITER [6], [7], and therefore a detailed assessment of the LH power deposition and CD efficiency in plasma conditions as close as possible to those expected in the ITER SS scenario is required [8], [9].

For the Steady State (SS) scenario in ITER substantial amounts of off-axis current drive will be needed to sustain a low magnetic shear over a broad region in the plasma core. Extensive studies on the feasibility of LH to maintain the ITER SS scenario have been recently published [2]. This paper discusses the predicting capabilities of existing numerical codes and summarises a number of observations from various LH systems on different fusion devices. The study also highlights that LH waves exhibit a reduced penetration at higher density, which might have an impact on the applicability of this CD scheme during the main heating phase.

A large group of numerical codes used to compute the absorption and CD are based on a combination of Ray Tracing/Fokker-Planck (RT/FP) solvers [11], [12], [13], [14], [15]. An alternative approach also includes the Wave Diffusion / FP model [16]. A thorough benchmarking of the most comprehensive codes available up to date in conditions close to ITER SS scenario reveals [17] not very consistent power deposition profiles and discrepancy between CD efficiency predictions.

Whilst the location of the LH power deposition in such conditions is consistently reproduced by the tested codes there is some disagreement between the computed profiles' shapes and non-negligible difference in the predicted total LH driven current [17].

A number of attempts to validate experimentally the numerical tools have been reported in the literature. Studies include the measurement of hard X ray spectra by the energetic fast electrons [12], [18], [19], the application of modulated power [20] and the analysis of the EC emission spectra by energetic electrons [10], [21]. Recent experimental observations [2], [10], [19], [20] conclude that at higher density the power deposition and CD profiles are broader and more off axis than the predictions by the available codes.

LH waves interact with supra-thermal electrons with velocities at least 3 to 4 times higher than the thermal velocity by Landau damping thus creating asymmetry in the Electron Distribution Function (EDF) in a direction parallel to the confining magnetic field. The fast electrons affect the Electron Cyclotron Emission (ECE) measurements and this has been recognised as a limitation to the applicability of this diagnostic during LH operation [22]. Nevertheless, the ECE data can still be used to assess the amount and the energy of the fast electrons created by the LH waves as we will show below. Essential deductions regarding the parameters of LH-generated fast electrons can be made by finding a consistent match between the measured and calculated ECE intensity. A number of studies address this issue [10], [21]. In all these cases the measured EC emission is used to constrain the calculated EDF, which is a superposition of a Maxwellian and drift-Maxwellian (MdM) distribution function as the latter accounts for the fast electron population. The study here uses similar approach but the main goal is to achieve a better consistency between the 'natural' EDF, which is the solution of the FP equation and the MdM EDF, which is used in ECE calculations. This approach clearly can not resolve completely the EDF over the whole plasma volume; however it can tell whether certain fast electron populations can produce the observed EC emission.

The JET experimental programme dedicated a number of sessions to the development of the SS scenario [23], [24] in which LHCD was used to drive off-axis current during the pre-heat and the main heating phase. Investigation of the power deposition by means of modulated LH power led to the conclusion that during the high-density main heating phase almost no LH power penetrates in the core [23], [24]. These studies however excluded the peripheral part of the plasma as the results could not be interpreted due to the smaller optical thickness there and also the ECE data were hugely affected by Edge Localised Modes (ELMs). The ECE measurements are now however further analysed in order to assess the LH power absorption and fast electron population in the plasma periphery. Obviously the method of analysis described here can not resolve EDF in full – such a task would require a far more comprehensive approach and would benefit significantly by constraining the analysis to the oblique ECE measurements. However, an estimate of whether the EDF has high-energy plateau in parallel direction can be done based on the existing standard ECE diagnostic measuring the emission in perpendicular direction.

The results reported here provide a further insight into the LH wave penetration and absorption

especially in high-density plasmas with line averaged densities from 3-3.5 $\times 10^{19}$ m^{-3} up to 5.5-6 $\times 10^{19}$ m^{-3}, which is of the order of the ones foreseen for the ITER SS operational scenario. The study also confirms that the presence of fast electrons in the plasma can be assessed from the ECE measurements at optically thin frequencies.

The paper is organised as follows. Section 2 discusses the experimental set-up and special attention has been paid to the relevant ECE diagnostic. The basic physics of LH wave penetration accessibility and absorption are also briefly described in Section 3, while the EC emission physics is discussed in Section 4. The method of analysis is detailed in Section 5. The experimental observations are then used to study the emission from the plasma as a function of the plasma density and some of the SS scenario development experiments are analysed as reported in Section 6. Summary and conclusions are given in the last Section.

2. EXPERIMENTAL SETUP AND DIAGNOSTICS USED IN THE STUDY

2.1. ECE DIAGNOSTIC AT JET

The ECE diagnostic at JET [22] consists of three different instruments: a Michelson interferometer, a 96-channel heterodyne radiometer and an oblique Michelson Interferometer [21]. The Michelson interferometer measures the ECE in X mode in the frequency range from about 50 to 940GHz, with a spectral resolution of 10GHz. The radiometer can use a selection from 4 to 6 over 12 mixers, depending on the magnetic field, and covers the range from 69GHz to 207GHz with maximum of a 96 closely separated channels with 250MHz bandwidth and channel separation of 500MHz. In radial dimension this is equivalent to spatial resolution of about 0.01m-0.02m in second harmonic X-mode (2X-mode) and 0.03m-0.05m in first harmonic O-mode (1O-mode), while the temporal resolution can be adjusted to up to 0.2ms. By selecting the frequency range corresponding to either 2X-mode or 1O-mode the range in toroidal magnetic field from 1.6T to 4T can be covered.

The Michelson interferometer is absolutely calibrated by means of both cold and hot calibrated sources, while the radiometer is cross-calibrated to the Michelson interferometer. The Line Of Sights (LOS) for both diagnostics are parallel to the midplane, see figure 1, but at different heights: 0.35m for the Michelson interferometer and 0.133m for the radiometer. This introduces some spatial error when cross-calibrating the two diagnostics. Since for typical JET configurations the centre of the plasma is displaced upwards by typically 0.30m to 0.40m, the Michelson LOS is generally very close to the plasma centre, whilst the radiometer data usually have a 'gap' in the very core due to the up-shift of the magnetic axis.

In the studies presented here data from the heterodyne radiometer in 2X-mode are analysed as it features the best time and space resolution, smallest frequency overlap and instrumental function which is least affected by the experimental conditions, therefore when we refer to ECE measurements further on we mean ECE measurements by this diagnostic in 2X-mode. The reflection and the radiation scrambling, i.e. changing the polarisation of the emission after reflection from the walls, are treated by means of the corresponding coefficients, R and P respectively, which in our case are

taken from the literature [22], R=0.65 and P=0.32 for the inner and outer wall of the vessel and R=1.0 and P=0.0 for the high field side cut-off. In the small optical thickness limit one should take into account multiple reflections from the wall as the forward and backward radiation contributes to the total emission detected at the vessel port. In this case the multiple reflections are treated in a more comprehensive way as discussed in [25].

It is important to mention that the ECE diagnostic measures the radiative temperature, Trad, as a function of the frequency. In optically thick plasmas Trad=Te and the temperature profile is derived after mapping the magnetic field on the radial co-ordinate. Inaccuracies in magnetic field measurements introduce an error in the determination of the cyclotron frequency and hence an error in the radial co-ordinate for the measured Te profiles. It has been assessed [26] that assuming about 1% increase in the experimentally measured magnetic field produces more consistent ECE profiles. In the study here we include this correction as this provides a reasonable match of the HFS and LFS profiles and also gives a better agreement between the ECE data and data from Thomson Scattering (TS) diagnostic. The errors in the ECE data are assessed to be of the order of 15% but slightly higher values (≈20%) can be assumed due to the calibration procedure.

The High Resolution TS (HRTS) was not available during all the pulses and in this case TS measurements based on the LIght Detection And Ranging (LIDAR) technique were used. It was also found that the emission spectra are very sensitive to the edge profiles of n_e and T_e and for that reason the data were compared to the edge LIDAR diagnostic as well. All these diagnostics have their own LOS and during the mapping procedure an error in the radial position is introduced due to the inaccuracy in magnetic diagnostics and equilibrium reconstruction.

In the study all radial profiles are mapped on the LOS of the radiometer marked as R_a. The main advantage in using R_a is that this is the natural co-ordinate of the diagnostic utilised in the experimental data interpretation hence the latter are not affected by the inaccuracy related to the mapping procedure: if the plasma midplane co-ordinate or toroidal/poloidal flux radius is used it would require mapping of all diagnostics, including the ECE, which will introduce additional errors.

2.2 LH SYSTEM AT JET

The LHCD system at JET is described in details in [27], [28]. The system is capable of launching maximum about 6MW in L-mode plasmas at 3.7GHz. At high-density H-modes the available LH power is slightly lower due to coupling issues; in most of the experiments presented here the coupled power was of the order of 2MW. The spectrum of the launched LH wave, expressed as a function of the RF power on the parallel refractive index $N_{||}$, can be changed by phase shifting the power delivered by each klystron. When the phases of the klystrons are selected so that there is no phase shift between adjacent multijunctions at the launcher mouth the spectrum can be presented as a narrow Gaussian curve peaked at $N_{||} = 1.84$. Some of the experiments in SS scenarios at JET are performed at different launching spectrum, $N_{||} = 2.1$ or $N_{||} = 2.3$, achieved by a phase shift at the launcher of 45^o and 90^o respectively.

3. PROPAGATION AND ABSORPTION OF LH WAVES

The absorption of the LH waves is discussed here in terms of a simple LH propagation model [16], [18], [29]. Although this model does not include FP calculations it helps understanding the physics of the LH propagation and absorption and underlines the main dependencies.

The LH wave can propagate in the plasma if the conditions $Re(N_r)>0$ and $N_{||} > N_{||acc}$ are fulfilled. Here N_r and $N_{||}$ are the radial and parallel component of wave refractive index with respect to the equilibrium magnetic filed. The first condition is required to assure that the LH wave propagation is allowed and determines upper and lower boundaries in the $N_{||}$ domain, $N_{||-} < N_{||} < N_{||+}$, where $N_{||-}$ and $N_{||+}$ are also known as upper and lower caustics. The second condition is the accessibility condition and sets a lower limits for $N_{||}$ in each region of the plasma. In this study the electromagnetic dispersion relation is used to determine the values of $N_{||-}$, $N_{||+}$ and $N_{||acc}$ for the cases of interest.

These constraints can be further used to assess the $N_{||}$ domain for which wave propagation is allowed in certain region in the plasma. LH waves are also damped very strongly for $N_{||} \geq N_{||abs} = 6.5/\sqrt{T_e}[keV]$. The latter condition is derived from FP calculations and is directly related to the well-known approximation for the origin of the plateau in the EDF, $v_{||}/v_{te} \approx 3.5$, where $v_{te} = \sqrt{T_e/m_e}$ is the electrons' thermal velocity. The strong wave absorption limit, $N_{||abs}$, will be used to provide an estimate of the location of the LH deposition. Moreover, as noted in the literature [29] the maximum of the power deposition is generally expected to be localised in the vicinity of the $N_{||+}$ and $N_{||abs}$intersection point.

The constraint on $N_{||}$ discussed above can be easily transformed into constraints for the LH wave phase velocity in parallel direction, v_{ph}, by the expression $v_{ph}/c = 1/N_{||}$. Adopting this notation, the wave-plasma interactions will take place according to the Landau damping condition for particles with parallel velocities $v_{||} = v_{ph}$.

The profiles of $N_{||+}$, $N_{||abs}$ and $N_{||abs}$ for two JET pulses at low and high density and the corresponding $v$ph/c profiles versus Ra are shown in figure 2.

The low-density case, figure 2a, clearly allows for a broader range of $N_{||}$ values over the whole plasma. Also in this case the accessibility, $N_{||} > N_{||acc}$, does not prevent waves with $N_{||} = 1.84$ to penetrate into the plasma core, whilst at high density, figure 2b, propagation for $N_{||} = 1.84$ is only allowed on the High Field Side (HFS) or in the plasma periphery on the Low Field Side (LFS). For the LH waves to be able to penetrate to the plasma core from LFS the waves need up-shift in the $N_{||}$ spectrum. The $N_{||+}$ and $N_{||abs}$ intersection point occurs in the region v/c»0.1 in the plasma periphery on the LFS and $v/c = 0.25-0.3$ in the core region. This evaluation provides an estimate of the $v_{||}$ range of the resonant electrons and it will be further used to assess the related CD efficiency.

4. EMISSION BY ELECTRONS GENERATED BY LH WAVES

4.1. EC EMISSION, TRANSPORT OF RADIATION AND GENERAL DEPENDENCIES

In order to diagnose the electron temperature, T_e, in a Maxwellian plasma one should measure the intensity of the EC emission, I_ω, providing the optical thickness τ_0 of the plasma at the measured

frequency ω is large enough.

The intensity of the emission passing through an emitting and absorbing medium can be calculated by means of Kirchhoff's radiation transport equation [30].

$$n_r^2 \frac{d}{ds}\left[\frac{I_\omega}{n_r^2}\right] = \beta - \alpha I_\omega \tag{1}$$

where α is the absorption coefficient, β is the emission coefficient while n_r is the refractive index throughout the propagating trajectory and is usually close to 1. The radiative temperature T_{rad} and the optical depth τ(s) over the observation path s can be defined as:

$$T_{rad} = \frac{8\pi^3 c^2}{\omega^2}\frac{1}{n_r^2}\frac{\beta}{\alpha}, \tau(s) = \int_0^s \alpha(s')ds' \tag{2}$$

The expression for the radiation transport can be further simplified by integrating (1) over the ray path thus deriving the equation for the emission from the plasma volume V and length in the observation direction L:

$$I_\omega = I_{\omega 0}e^{-\tau_0} + \frac{\omega^2}{8\pi^3 c^2}\int_0^L T_{rad}(s)\alpha(s)e^{-\tau(s)}ds, \quad \tau_0 = \tau(L) = \int \alpha(s')ds' \tag{3}$$

where $I_{\omega 0}$ is the intensity of the incident emission and τ_0 is the optical thickness of the entire plasma; the direction of integration in (2) and (3) is from the observation point towards the opposite boundary of V. For a Maxwellian distribution with relaxation temperature, T_e, it can be shown that the coefficients α and β are related via $\beta = (T_e\omega^2/8\pi^3c^2)\alpha$, so that from (2) it follows $T_{rad} = T_e$.

Assuming that the acquired temperature Te does not change significantly over L and there is no incident emission, i.e. $I_{\omega 0} = 0$, the emission intensity, I_ω, relates to T_e as

$$I_\omega = \frac{\omega^2}{8\pi^3 c^2}T_e\left(1 - e^{-\tau_0}\right) \tag{4}.$$

Providing that the plasma is optically thick, i.e. $\tau_0 >> 1$, (3) reduces to $I_\omega = \omega^2/8\pi^3c^2$. The latter expression is only valid if all the conditions discussed above are met, i.e. plasma should be optically thick for the measured frequencies with Maxwellian EDF and with sufficiently small radial changes of T_e.

The experimental conditions in tokamaks are however different from the ideal case; the magnetic field, the density and the electron temperature are not constant. The plasma is also not optically thick for certain frequencies in which case the EC radiation passes a number of times through the plasma bouncing from the inner and outer walls. Moreover the velocity distribution of the electrons in the plasma may deviate from a Maxwellian distribution, e.g. in presence of a non-negligible amount of fast electrons generated by the LH waves. All these factors can affect the EC emission and the T_e values derived from the ECE measurements can significantly deviate from the real T_e values.

4.2. EC EMISSION IN PRESENCE OF FAST ELECTRONS

In the presence of fast electrons and with a non-Maxwellian EDF, T_{rad} differs from T_e and the methodology of temperature measurements given above needs to be modified. The measured ECE intensity now contains a significant contribution from the fast electrons and this is more pronounced for frequencies with small optical thickness for which $\tau_0<1$.

An account of the impact of the fast electrons on the ECE measurements is schematically given in figure 3 in which the radial profiles of the 1st, 2nd and 3rd harmonics of the ECE are shown together with the cut-off and upper hybrid frequency. Shown also are the optically thin and thick region, an example area dominated by the LH-generated fast electrons and four particular cases of EC emission by them. In general the fast electrons will radiate at frequency smaller than their cyclotron frequency, so called downshifted emission, and this will have a negligible impact on the ECE data if the downshifted frequency, ω/γ_0 where $\gamma_0 = 1/\sqrt{(1-(v_0/c)^2)}$, is in the optically thick region, (see e.g. the vertical arrow 3 in figure 3). However, there will be a significant impact on the ECE intensity in case of a large amount of fast electrons in the optically thin region (see e.g. vertical arrow 1), or for electrons in the optically thick plasma region but whose downshifted emitted frequency is in the optically thin region, as indicated by vertical arrow 2. As a result of this a peculiar 'tail' with high T_e values will form in the measured T_e profile near the edge. Another important contribution will come from the downshifted third harmonic frequency, which in most cases at JET is optically thin. The third harmonic downshifted by the fast electrons, as e.g. indicated by the vertical arrow 4 in figure 3, will also affect the HFS measurements.

5. THEORETICAL BACKGROUND AND METHOD OF ANALYSIS

5.1. EDF WITH BULK AND DRIFT MAXWELLIAN

A number of numerical methods to compute the EC emission and solve the radiation transport equation in Maxwellian plasma with a small fraction of fast electrons exist in the literature [31], [32], [33]. In general, the calculation of the emissivity and absorption requires solving the dispersion relation near the 2nd EC harmonic for 2X-mode or near the 1st harmonic for 1O-mode to obtain the complex wave vector, $\boldsymbol{k = k' + ik''}$, and the relevant dielectric tensor elements, $\varepsilon_{ij} = \varepsilon^h_{ij} + i\varepsilon^a_{ij}$ with contributions from Hemitian ε^h_{ij} and anti-Hemitial parts ε^a_{ij}. The EDF in presence of fast electrons can be approximated by a superposition of a Maxwellian and a plateau distribution in parallel direction. In this study the plateau is modelled by a drift Maxwellian characterised by a parallel drift velocity v_d and drift temperature T_d. A full relativistic treatment is used so that the Maxwellian and drift Maxwellian (MdM) EDF can be presented as:

$$f = (1-\eta) f_b + \eta f_d = (1-\eta)\frac{\mu_b}{4\pi K_2(\mu_b)} e^{-\mu_b \gamma} + \eta \frac{\mu_d}{4\gamma\pi_d^2 K_2(\mu_d/\gamma_d)} e^{-\mu_d(\gamma - p_\parallel v_d/c)} \qquad (5)$$

where $\gamma = \sqrt{(1+p^2)}$ is relativistic factor and p is the relativistic moment normalised to $m_e c$, γ_d is determined from the shift of the drift as $\gamma_d = 1/\sqrt{(1-(v_d/c)^2)}$, K2 is the modified Bessel function of

the second kind with argument $\mu = m_e c_2/T$ where the subscripts b and d refer to the bulk or drift temperature respectively. In equation (5) $\eta = n_{ef}/n_e$ is the ratio of the fast electrons density to the plasma density. The EDF modelled in such a way retains its lowest order moments if the bulk temperature is selected as $T_b = T_e$ and the concentration of fast electrons is small, $\eta = n_{ef}/n_e << 1$. The latter and the drift velocity vd determines the driven current density j_d as $j_d = e\ n_e\ \eta\ v_d$.

The dielectric tensor elements e_{ij} in this case are the sum of the contributions from each distribution function. Further, the modified Maxwellian distribution is treated as moving in a co-frame and the dielectric tensor elements are converted to elements in the laboratory frame using the Lorentz transformation. The radiative temperature thus can be found by Lorentz transforming Kirchoff's law and details of the whole procedure can be found in [32].

Although such an approximation does not always fit well to the EDF with a plateau as calculated by the FP code its greatest advantage is that it allows for an easy and relatively accurate calculation of the EC emission. It has been shown in [32] that the EC emission from an EDF as the one in (5) is a combination of the emissions by both: the bulk and the fast electrons and the radiative temperature in the case of observation in perpendicular direction can thus be presented as:

$$T_{rad} = \frac{\alpha_b T_b + \alpha_d T_d / \gamma_d}{\alpha_b + \alpha_d} \tag{6}$$

where $\alpha = 2\mathrm{Im}(k_\perp) = 2k''$, α_b is due to the bulk electrons and α_d is the contribution due to drifted tail of the EDF. In the case of 2X mode the bulk and drift contributions α_b and α_d are calculated by means of the relevant dielectric tensor elements.

Although the described procedure allows for a quick calculation of the EC emission and the driven current, in general it does not allow matching the real distribution function as derived from FP calculations with the main differences between the MdM and the FP solutions in the region of the quasilinear plateau. Special attention has been paid in the study to cases with large discrepancies between both.

The FP calculations [34] use the values of the normalised quasi-linear diffusion coefficient, D_0, the low velocity limit, $w_1 = v_{\|}/v_{th}$, and the width of the plateau, Δ, to determine the EDF evolution when LH waves are absorbed in hot plasma. In order to obtain consistency between the MdM EDF and FP results it is necessary to relate D_0, w_1 and Δ to the MdM parameters, namely η, T_d and v_d. One possible way of doing this is to fit the MdM EDF as given by equation (5) to FP solutions with fitting parameters η, v_d and T_d. However, there are at least two issues, which restrict the quality of such fit: (i) it assumes that D_0, w_1 and Δ in the reference FP solution are well known, and (ii) the MdM EDF can not reproduce the plateau correctly especially near the two velocity boundaries of the plateau, i.e. at w_1 and $w_1 + \Delta$.

In order to illustrate the discrepancies the so called parallel distribution function $F_{\|}(p_{\|})$:

$$F_{\|}(p_{\|}) = 2\pi \int_0^\infty p_\perp f(p_\perp, p_{\|}) dp_\perp \tag{7}$$

is calculated for MdM and FP EDF and both are compared. In the study we use a FP code as the one described in [34] with the following parameters: effective charge $Z_{eff} = 1.5$, normalised electric field $E_{norm} = E\, e/m_e v_{th} \nu_{te} = 0.002$, normalised quasilinear diffusion coefficient $D_0 = DQL/v_{th}^2 \nu_{te}$ in the range 0.2 to 0.02, plateau origin $w_1 = 3.5$ and width Δ in the range 2 to 8. In the notations above D_{QL} is the quasilinear diffusion coefficient, nte is the thermal collisional frequency while all the other symbols have their usual meanings. The values of Z_{eff} and E_{norm} were selected in order to be close to the measured values in the experiments of interest, while the electron temperature Te was varied between 0.5keV and 2keV.

Not all combinations of η, T_d and v_d parameters produce MdM EDFs compatible with FP solutions and this is an essential issue in the analysis performed here. In order to assess what would be a realistic range of these parameters different types of fits to the FP EDF were studied, and selected results are shown either as a contour plot of $f(p_\perp, p_\parallel)$, (see figure 4a and c), or as $F_\parallel(p_\parallel)$ plots (see figure 4b and d). We were not able to reproduce the EDF with a large plateau using a direct fit, as illustrated in figure 4a and 4b. The second fitting method we used consisted in removing the Maxwellian bulk from the FP result and fitting only the remaining non-Maxwelian part. The results are shown in figure 4c and 4d. It reproduces better the large plateau and reasonably well the normalised driven current, however this reasonably good agreement could only be achieved for $T_e \geq 1$keV and reference FP EDF with D0³0.05 and moderate values of $\Delta \geq 4$.

A scan of the electron temperature is shown in figure 5. The fits to the FP results with $\Delta = 6$ are done by removing the bulk from the FP EDF and fitting the plateau to a drifting Maxwellian, while for $\Delta = 2$ the direct fit results are shown. Although the latter appear to match better the FP result (at least visually), it was found that the direct fit is incapable of matching the amount of the driven current. In general the MdM EDF reproduces better the FP result for sufficiently high T_e as it was found that FP EDF at low Te and with large plateau is almost impossible to be modelled by MdM. Also in all cases the EDFs differ in the region near w_1 and $w_1 + \Delta$, i.e. the low and the high velocity limits of the plateau, as MdM EDF is always smaller than the FP results. In contrast, the MdM EDF has a distinctive bump in the middle of the plateau, which is inconsistent with FP calculations, as illustrated in figure 5.

A summary of the fitted EDF and the parameters of the MdM for $T_e = 0.5$, 1 and 1.5keV and $\Delta = 2$ and 6 is given in Table 1. The table shows that the FP and MdM results for j_w and j_d only slightly differ. Note that a good consistency between p_C and p_{EE} has been obtained as well, and we conclude that p_C and p_{EE} can be used as additional reference quantities when comparing the FP and the MdM EDF.

5.2 METHOD OF ANALYSIS

The analysis presented here aims at finding the profiles of fast electrons density, h, temperature, Td, and velocity vd for which the calculated ECE spectra match the measured data. In addition a number of constraints to these parameters and the resulting MdM EDF are imposed in order to ensure a consistency with the physical processes being involved.

The mismatches between MdM EDF and FP results, described in the previous Section, add to the problem that the real FP EDF is unknown therefore extra constraints were introduced in the study in order to improve the confidence in the results. First, the MdM predicted current density jd and total driven current Id were used to set limits on h and vd/c. The most obvious one is that Id should not exceed the total plasma current, IP. It is also assumed that in H-mode the plasma current at the pedestal region is determined mainly by the bootstrap current and jd should not exceed it. This assumption is supported by recent theoretical studies and modelling of JET pulses [35] which indicate that ELM behaviour in H-mode JET plasma is determined by the pressure gradient and the current density (via the magnetic shear) at the pedestal. Simulations of the most interesting cases discussed here show that CD as large as the bootstrap current at the pedestal region will change substantially the ballooning and peeling-mode stability conditions at the plasma edge, which in turn will be accompanied by changes in the ELMs behaviour. Although the experiments discussed here did not aim to study this aspect of the problem, in general no significant changes in the ELMs amplitude and frequency were observed in the cases when the LH power was accidentally dropped or turned off. Based on these observations it can be concluded that the relatively unchanged ELM behaviour while varying the LH power can be merely interpreted in terms of small changes to the pedestal current density.

Another constraint that can be implemented is to take into account the total coupled LH power, P_{LH}, which can be related to the calculated absorbed LH wave power density, p_W. The consistency between p_C and p_{EE} (see table 1), and the fact that these two quantities represent the same physical quantity, i.e. the power needed to form and sustain a plateau (or a drift Mawellian distribution) in a hot plasma, justifies the use of p_{EE} to assess p_C. Moreover, assuming that the Ohmic heating contribution is negligible in comparison to p_W and p_C, the power balance gives $p_W \approx p_C$ so these two quantities should be approximately equal in steady state regime. When the FP and MdM EDF result are consistent one can summarise $p_W \approx p_C \approx p_{EE}$. Integrating all three quantities over the plasma volume will provide the total power P_{EE} as a rough estimate of total absorbed LH wave power, P_W, which can be compared to the measured coupled power, P_{LH}, and thus one can straightforwardly use this as a constraint in the analysis. In the studies presented here the power p_{EE} is calculated by means of the same FP solver after evaluating the linearised collision operator $C((1-\eta)f_d, \eta f_b)$ which can be expressed in terms of flux functions, $\mathbf{S_{EE}}$ [34]. The latter provides an easy way of computing the collisional power density after integrating the product $me\boldsymbol{\nu}.\mathbf{S_{EE}}$ in the velocity space.

The extent to which the fast electrons' parameters influence the radiative temperature can be found from equation (6). For optically thin frequencies, i.e. with the 2nd harmonic resonance near the edge, T_{rad} has to be integrated over the observation path, in order to obtain the apparent EC emission. The integration is performed according to equation (3) until the intensity of the emission reduces to a sufficiently low level, while multiple reflections from the walls are taken into account by means of the relevant formula [25]. The values of the electron temperature calculated following this procedure were then used in a fit to the experimental data. In order to find the best set of η, T_d

and v_d profiles we used a least square minimisation between the measured and modelled ECE data in the optically thin region.

Although the pulses of interest were analysed individually in a slightly different manner in general the method of analysis can be described as follows. Initially minimisations aiming at localisation of the deposition have been performed by varying the boundaries of the deposition profile. The fitting parameters were η, T_d, and vd with constant profiles, while the Sum of Squared Errors (SSE) between the measured and calculated data was used as a measure of the goodness of the profile. The outer part of the absorption region was found to be near the separatrix, while locating the inner boundary was more difficult especially in the cases of broad deposition covering the plasma core. As illustrated in figure 3 by the vertical arrow 3, the downshifted emission in this region is fully re-absorbed by the thermal electrons on the LFS so that the ECE data does not contain information about the fast electrons there. This problem is partially solved by imposing the constraint $P_{LH} \approx P_{EE}$ as discussed in the previous paragraph. This constraint, however, has to be very carefully used in H-mode plasmas because of possible contributions of non-thermal background emission to the ECE measurements. Once the boundaries of the absorption region were found and fixed, the next step in the analysis was to check for possible modifications to η and T_d profiles by performing another fit to the measured data. It was found that at low density an increase in η and T_d in the outer part of the deposition match even better the experimental results. In this case again the solutions were subject to a number of constraints involving the absorbed power, the current drive and the MdM EDF. The latter was compared to the FP solutions and the cases with significant discrepancies were discarded.

In assessing the uniqueness of the solutions for η, T_d, and v_d, a large set of fast particle profiles was studied and we found that the EC emission in the optically thin edge is very sensitive to the values of η and T_d and to a lesser extent to v_d. The procedure described above results in reliable η and T_d profiles and somewhat reduced precision for the v_d profile. However, the later affects only the estimate of the CD while in the study we focus on the absorption profile evaluation. In some of the examples shown below, especially in cases when the calculated EC emission is found to be fairly insensitive to v_d, we assume vd/c of the order of 0.1. This value of v_d/c is consistent with the wave propagation model discussed in previous Section for low- and high-density pulses as shown in figure 2.

6. ECE EMISSION FROM JET PLASMAS

The method of analysis of the ECE data described above was initially checked for reference Ohmic pulse where a good agreement between the experimental and calculated ECE profiles was found for both optically thick and optically thin frequencies. In what follows we describe the results obtained in various H-Mode plasmas in JET.

6.1. H-MODE REFERENCE WITHOUT LH POWER

The experimental profiles and the results obtained in modelling the JET H-mode high-density Pulse

No: 78052 at 2.7T/1.8MA are shown in figure 6a and 6b. The calculations match the measurements reasonably well for all the optically thick frequencies, i.e. larger than 118GHz. However, the experimental and theoretical data differ at the edge where the optical thickness is small.

For frequencies of 115.4GHz and 115.7GHz with corresponding 2nd harmonic EC resonances at Ra»3.88m and Ra»3.90m respectively, both locations well into the shadow of the limiter as shown in figure 1, the code predicts almost zero emission while the measurements give about 600eV. An ECE intensity of the order of 0.5-1keV at optically thin frequencies outside the plasma volume is an indication of some background non-thermal emission. Indeed the discrepancy between the measured and simulated data can be resolved by adding small amount of fast electrons, h»0.0023 and Td»5keV, near the separatrix, as shown in figure 6. The presence of a fast electrons population near the plasma boundary has been observed in several other cases [36], [37], [38]. The non-thermal background emission at optically thin frequencies in H-mode and the origin of the causative fast electrons, further on called non-confined fast electrons, and the conditions at which they are present together with some estimates of the necessary transport coefficients are discussed in detail in [36]. The implications for our analysis are that distinguishing between non-confined fast electrons and fast electrons created by the LH waves will be more difficult especially if they have similar concentration and temperature. For that reason the plasmas in H-mode are analysed at different levels of the applied LH power with a first time slice taken when $P_{LH} \approx 2$MW and a second when PLH is very small or zero.

6.2. DENSITY SCAN AT 3.4T L- AND H-MODE PLASMAS

The analysis was initially performed on the low-density L-mode 3.4T/1.5MA JET Pulse No: 77609. Profiles are taken at 16.4s and slightly smoothed as shown in figure 7a. Figure 7b shows the results of the simulated ECE spectra compared to the experimental one.

In order to match the relatively flat emission intensity between 140GHz and 146GHz non-monotonic increasing towards the edge h and Td profiles were used. With $\eta = 0.0006$ and $T_d = 21$keV for $R_a = 3.07$m to about 3.50m and monotonically increasing η and T_d from 3.50m towards the edge. The fast particle concentration h increases 3 times to up to about $\eta \approx 0.002$ while T_d reaches about 30keV at 3.74m. The emission is not very sensitive to the values of v_d/c so in this case 0.1 was selected in agreement with discussions in Section 3 and figure 2a. For these values of the fast electron concentration η and drift velocity v_d/c a current profile j_d peaks at the periphery, as shown in figure 7a, and a total current I_d of about 180kA was derived. The total energy exchange rate PEE from the MdM EDF is estimated to be about 1.8MW, which is in a good agreement with the total launched LH power, $P_{LH} = 2$MW. The uncertainties in the jd and Id assessment reflect the uncertainties in vd/c values.

The high-density H-mode 3.4T/1.8MA Pulse No: 77616 was analysed at 16.92s when 1.85MW of LH power was applied. The kinetic profiles are shown in figure 8a.

The fast electrons profiles η and T_d used in this case were narrower and situated more off-axis. In

addition to this η and T_d were non-monotonic starting with constant values of 0.00025 and 8.5keV between 3.53m and 3.80m and rise very sharply to about 0.0006 and 19keV at 3.84m, figure 8a. The driven current in this case is about 82kA for $v_d/c = 0.1$. The energy exchange rate P_{EE} is about 1.6MW, half of which is a contribution from LH generated fast electrons between 3.53m and 3.72m. Due to the significant non-thermal background emission from the pedestal region, 3.72m to 3.84m, this value of P_{EE} has rather large error bars and can not be used as a constraint in this case.

As it was discussed in the previous Section, in H-mode enhanced emission from the edge is observed for optically thin frequencies. Therefore, the EC emission has been checked by analysing the non-LH phase of Pulse No: 77616 at 17.32s. In this case the EC emission at the edge was small and was reproduced by $\eta = 0.00022$ and $T_d = 7.5$keV in the narrow region between 3.72m and 3.84m. It can be concluded that the measurements of enhanced ECE during the LH phase are due to (i) fast electrons generated by LH in the region 3.53m to 3.72m; and (ii) superposition of non-thermal background emission and fast electrons generated by LH waves in the region 3.72m to 3.84m. It is worth mentioning that although the two pulses, Pulse No's: 78052 and 77616, were in H-mode they were very different regarding equilibrium and electron temperature at the pedestal region: i.e. 0.02m inside the separatrix, we find 1.1keV in the first case and 0.7keV in the second. This difference can partially explain the much smaller values of h (about 10 times smaller) in the non-LH phase of Pulse No: 77616 in comparison to Pulse No: 78052.

The LH deposition and CD assessed from the ECE data via the described method for three different densities in 3.4T/1.8-1.5MA JET Pulse No's: 77609, 77612 and 77616 are given in figure 9. The CD profiles are calculated for vd/c=0.1 and are found to shift to the edge with increasing density, which is in agreement with previous studies on the subject [20]. Provided that the fast electrons drift v_d/c is the same for all three cases, the total driven current drops about 2.2 times from the lowest density case to the highest one. This observation is also in qualitative agreement with the recent analysis of the LH absorption and CD efficiency. In comparison the RT/FP code used at JET [13] gives more central deposition profiles for the three cases and overestimates the total current drive 3.5-4.5 times.

6.3. H-MODE SS SCENARIO DEVELOPMENT PULSES

The development of the SS scenario at JET [23], [24] required the implementation of different techniques to control the plasma current profile evolution in the ramp-up and during the flat-top phase and LH was anticipated as being a good tool to achieve this. The LH penetration and absorption in these experiments has been investigated [2] and here further details are presented and discussed on a plasma with poor and with improved penetration.

The pulses investigated are at 2.7T/1.8MA and the first one, Pulse No: 72829, has flatter density profile and lower temperature with central values of $n_{e0} \approx 5.5\times10^{19}m^{-3}$ and $T_{e0} \approx 4$keV. The profiles at 6.04s when LH power of 2.0MW was launched with N||=1.84 are given in figure 10a. The results of the modelling and comparison to the experimental ECE data are provided in figure 10b.

At first an optimisation procedure based on finding the best match between experimental and

modelled ECE data in the optically thin region, i.e. for the five outermost frequencies from 115GHz to 117GHz in figure 10b, has been performed. A good fit between experimental and calculated ECE data was found assuming a narrow deposition profile, i.e. from 3.78m to 3.82m, and $\eta = 0.0024$, $T_d =$ 3.9keV and $v_d/c \approx 0.13$. For these values of fast electrons' parameters the power P_{EE} was assessed of the order of 4MW, while the averaged LH driven current density is about $j_d \approx 400 kA/m^2$. This value is rather large and it was found to be inconsistent with the assumption that the LH driven current does not dominate the pedestal current density, which is estimated to be of the same order. It was found, however, that this deposition profile is less sensitive to the MdM drift velocity, as a broad range of possible vd values produced reasonably good data. Therefore, the next step in improving the consistency between MdM and experimental observations was to use this deposition profile and to reduce the values of h and vd, while increasing Td.

The ECE measurements were reproduced well, as shown in figure 10b, assuming MdM EDF with $\eta = 0.00125$, $T_d = 5.5$keV and $v_d/c = 0.01$ in the region between 3.78m and 3.82m. The uncertainty in vd is large and different values of v_d/c were tested. The best match was found for $v_d/c = 0.01$, as shown in figure 10b. The driven current for $v_d/c = 0.01$ is calculated to be Id»9kA while the averaged CD density is about $j_d \approx 17 kA/m^2$.

In order to assess the non-thermal background emission, the same pulse, Pulse No: 72829, is modelled later on at 9.18s, when the LH power was turned off. As a result the ECE intensity dropped by 20% to 30%, as seen on figure 10b by the grey '+' symbols, although the pedestal and the core did not change significantly. The ECE emission at this time slice was reproduced assuming smaller values of $\eta \approx 0.0008$. The fast electron temperature T_d was essentially kept the same, while for v_d/c zero values were used. Based on these results it can be concluded that the LH power turn off results in only 36% decrease of h. The fact that the EC emission changes very little with LH power and it can be reproduced only by small increase of fast electrons concentration near the pedestal, $3.78m < R_a < 3.82m$, is an indication of poor penetration and absorption of the LH waves.

The other pulse, which was analysed was again 2.7T/1.8MA Pulse No: 72835 and it has a more peaked electron density and temperature profile with central values of $n_{e0} \approx 5.4 \times 10^{19} m^{-3}$ and $T_{e0} \approx$ 5.5keV. The relevant profiles are given in figure 11a. This pulse also differs from Pulse No: 72829 by a different $N_{||}$ of the launched LH power which in this case was $N_{||} = 2.3$. The total coupled LH power was 2MW at 6.93s and the power was tripped to about 0.6MW shortly after that.

As in the previous case initially the LH absorption region was assessed by means of optimisation procedure minimising SSE between the measured and modelled ECE data in the optically thin region, from 115GHz to 117GHz in figure 11b. Results of this procedure indicated broader LH absorption profile as the fast electrons were predicted between $3.72m < R_a < 3.81m$, figure 11a. The best match to the experimental data was found for $\eta \approx 0.0012$, $T_d = 7.3$keV and $v_d/c \approx 0.22$. The averaged CD density is $j_d \approx 380 kA/m^2$, which is again larger than the current density in the pedestal region assessed to be of the order of $300 kA/m^2$. Subsequently lower values of η and v_d/c were tried and reasonable match to the experimental data, figure 11b, was found for MdM with $\eta \approx 0.00079$, $T_d =$ 7.8keV and vd/c in the range 0.14 ± 0.02, figure 11a. For these values of h and vd/c the averaged j_d

was about 150kA/m^2 and the total current of $I_d \approx 150$kA is predicted. It has to be noted, however, that these values are naturally greater than the real LH current drive as the background non-thermal emission is not taken into account in this assessment. Numerical analysis of Pulse No: 72835 has been performed [2], [10] by a more comprehensive set of numerical codes, which includes C3PO-LUKE code and spectrum from the LH coupling code ALOHA. The latter accounts for the changes in the launched wave spectrum due to non powered klystrons. Although the calculated deposition was again more central than the profiles shown in figure 11a, the numerically estimated total current drive in this case was about 100kA [2]. This is 30% lower than the value given here, which shows good consistency between the calculated data and the results reported here.

In addition, a comparison between MdM EDF and FP solution has been done. The MdM EDF fits reasonably well to the FP calculations for 1keV and 1.5keV plasma with $D_0 = 0.04$ and $\Delta = 6$, figure 11c and 11d. For comparison, for the 1keV case in figure 11d the current predicted by the MdM EDF, j_d, is only 5% smaller that the current j_{LH} as calculated by FP. For the 1.5keV case, figure 11c, j_d is 20% lower than the FP result. This good agreement between EDFs provides additional confidence in the interpretation of the results.

The analysis was repeated at another time slice, 7.07s, when the LH power was tripped to about 0.6MW. Yet again the T_d and v_d/c profiles were kept unchanged as shown in the bottom graph of figure 11a while, the h parameter was reduced about twice to $\eta \approx 0.0004$. The current I_d is calculated to be about 75kA. The discrepancy between the amount by which the LH power was reduced, 70% down, and the change of h, which is about 50%, indicate possibly contributions from background non-thermal emission. A rough assessment assuming linear contributions from the LH-generated and non-confined fast electrons in the registered EC emission and constant non-thermal background emission can be made. Based on this assumption and the numbers given above the current estimate of 75kA during 0.6MW of LH power is overestimated twice due to the non-thermal background emission, while the current of 150kA at $P_{LH} = 2$MW as it has been assessed in the previous paragraph is overestimated by about 30% which is in even better agreement with the results in [2], [10]. In case the LH power is completely switched off the emission at the very edge, e.g. for f = 115.4GHz and f = 115.8GHz in figure 11b, does not drop to zero as predicted by the ECE calculations rather than measuring values of about 350eV and 450eV respectively. In addition, trials with non-confined fast electrons with parameters, $\eta = 0.0004$, $T_d \approx 8$keV and $v_d/c = 0$ in the region 3.77m to 3.81m, reproduce the edge ECE measurements in the non-LH phase, $P_{LH} = 0$, reasonably well. The MdM EDF in this case is shown by dash-dotted line in figure 11d and when compared to the LH generated tail, dashed line in figure 11d, one concludes that the non-confined fast electrons do not affect the plateau of the EDF. Besides in this pulse the non-confined fast electrons are located at the very edge, from 3.77m to 3.81m, while the region between 3.72m and 3.77m is clearly dominated by LH generated fast electrons. This is an indication of improved wave penetration in Pulse No: 72835 compared to the previous pulse, Pulse No: 72829.

For the purpose of the analysis performed here assessing the exact contribution by the non-confined fast electrons is not important as far as one can conclude that changes in the LH power

generate relevant changes in the fast electrons parameters. As shown in the both examples these changes affect globally the η parameter, i.e. η changes with LH power in the region $3.78\text{m} < R_a < 3.82\text{m}$ for Pulse No: 72829 and in $3.72\text{m} < R_a < 3.81\text{m}$ for Pulse No: 72835. One can conclude that in the second case the LH absorption region is slightly more inward and about twice broader. Comparing the kinetic profiles of the two pulses in the region $3.74\text{m} < R_a < 3.81\text{m}$ one sees that Pulse No: 72835 has lower and more peaked density, average value of $n_e \approx 2.8\times10^{19}\text{m}^{-3}$ compared to $n_e \approx 3.2\times10^{19}\text{m}^{-3}$ in Pulse No: 72829, and higher temperature, $T_e \approx 1.3\text{keV}$ compared to $T_e \approx 1.1\text{keV}$ in Pulse No: 72829. This conclusion suggests possible remedy regarding improving the LH penetration in high-density H-mode plasmas. Naturally one should provide lower pedestal density and higher temperature in the region just inside the separatrix. Higher $N_{||}$ used in Pulse No: 72835 could have an impact as well.

The estimated vd/c values in the two pulses discussed above were very different, $v_d/c \approx 0.01$ for Pulse No: 72829 and $v_d/c \approx 0.14$ for Pulse No: 72835, resulting in huge difference in the CD, which is about 9kA in the first case and 150kA in the second. The uncertainty in v_d/c assessment via the described analysis is large, as in some cases the computed ECE spectra are not very sensitive to this parameter. Even if equal values of v_d/c are taken one would have slightly larger CD in the second case merely due to the larger LH absorption region in Pulse No: 72835.

CONCLUSIONS

Observed enhanced EC emission at the plasma edge during application of LH power at JET is due to LH generated fast electrons. It has been shown that the measured EC emission can be used to assess the LH power deposition and to approximately estimate the LH driven current. Results confirm that an increase in the plasma density, as e.g. caused by the pedestal in H-mode plasmas, leads to a reduction in the penetration of LH waves. The absorption profiles are shifted to the plasma periphery while the current drive decreases with increasing density. The very peripheral absorption at high density can not be explained satisfactorily by the classical effect of wave accessibility as this effect has been accounted for in the tested codes. Nevertheless the numerical results indicate more central deposition than the profiles presented here.

Density scans of 3.4T/1.8-1.5MA JET pulses show that the total driven current by the LH waves with total coupled power of 1.6-1.8MW drops to about 82kA in H-mode compared to 183kA in L-mode conditions. The results from the numerical analysis of two 2.7T/1.8MA JET SS pulses indicate that changes in the pedestal conditions, i.e. reducing the density from $3.2\times10^{19}\text{m}^{-3}$ to $2.8\times10^{19}\text{m}^{-3}$ and increasing the temperature from 1.1keV to about 1.3keV, lead to twice broader LH power deposition accompanied by an improvement in the CD efficiency.

Based on these observations it can be concluded that the combination of lower pedestal density and higher temperature just inside the separatrix, and in addition possibly higher N||, improves the penetration of the LH waves. This could be a possible remedy for the future application of LH in high-density plasmas at conditions close to the ITER SS scenario. For ITER, this could come on top of the benefits from the use of 5GHz as LH frequency and the higher confinement magnetic field.

ACKNOWLEDGEMENT

This work was supported by EURATOM and carried out within the framework of the European Fusion Development Agreement. The views and opinions expressed herein do not necessarily reflect those of the European Commission. The work was also part-funded by the United Kingdom Engineering and Physical Sciences Research Council under grant EP/G003955.

REFERENCES

[1]. Fish N, 1987, Rev. Mod. Physics **59**(1), 175
[2]. Goniche M et al, 2010, Plasma Physics and Controlled Fusion **52**, 124031
[3]. Porkolab M, 1985, Wave Heating and Current Drive in Plasmas, eds. V Granatstein and P. Colestock, (Gordon and Breach Sci. Publishers, 1985), p.219
[4]. Mailloux J et al, 2002, Physics of Plasmas **9**, 2156
[5]. Challis C et al, 2001, Plasma Physics and Controlled Fusion **43**, 861
[6]. Hoang G T et al, 2009, AIP Conf. Proc. Volume 1187, pp. 411-419, Radio Freq. Power in Plasmas, 18th Top. Conf. on Radio Freq. Power in Plasmas
[7]. Hoang G T et al, 2009, Nuclear Fusion **49**, 075001
[8]. ITER Phys. Basis Expert Group, 1999, Nuclear Fusion **39**, 2495
[9]. Gormezano G et al, 2007, Nuclear Fusion **47**, S285
[10]. Goniche M et al, 2010, Proc. 37th EPS Conf. on Plasma Physics (Dublin, Ireland)
[11]. Bonoli P, Englade R C, 1986, Phys. Fluids **29**, 2937
[12]. Baranov Yu et al, 1996, Nuclear Fusion **36**, 1031
[13]. Esterkin A, Piliya A, 1996, Nuclear Fusion **36**, 1501
[14]. Cesario R et al, 2010, Nature Communication Aug 2010
[15]. Peysson Y, Decker J, 2007, AIP Conf. Proc. Volume 933, pp. 293-296, Radio Freq. Power in Plasmas, 17th Top. Conf. on Radio Freq. Power in Plasmas
[16]. Kupfer K et al, 1993, Physics of Fluids B **5**, 4391
[17]. Bonoli P, 2006, Proc. 21st Int. Conf. on Fusion Energy 2006 (Chengdu, China) (Vienna: IAEA) CD-ROM file IT/P1-2
[18]. Litaudon X et al, 1996, Plasma Physics and Controlled Fusion **38**, 1603
[19]. Wallace G M et al, 2010, Physics of Plasmas **17**, 082508
[20]. Kirov K K, Baranov Yu et al, 2010, Nuclear Fusion **50**, 075003
[21]. Sozzi C et al, 2009, AIP Conf. Proc. Volume 1187, pp. 387-391, Radio Freq. Power in Plasmas, 18th Top. Conf. on Radio Freq. Power in Plasmas
[22]. de la Luna E et al, 2001, Review of Scientific Instruments **74**, 1414
[23]. Mailloux J et al, 2009, Proc. 36th EPS Conf. on Plasma Physics (Sofia, Bulgaria)
[24]. Mailloux J et al, 2010, 23rd IAEA Fusion Energy Conference (Daejon, Republic of Korea)
[25]. Costley A E et al, 1974, Physical Review Letters **33**, 758
[26]. Barrera L et al, 2010, Plasma Physics and Controlled Fusion **52**, 085010
[27]. Pain M et al, 1989, Proc. 13th Symp. on Fusion Engineering (Knoxville, TN)
[28]. Lennholm M et al, 1995, Proc. 16th Symp. on Fusion Engineering (Champaign, IL)
[29]. Dumont R et al, 2000, Physics of Plasmas **7**, 4972
[30]. Bekefi G, 1966, Radiation Processes in Plasma, J. Wiley and sons, inc., N.Y. London Sydney

[31]. Fidone I, Granata G et al, 1980, Physics of Fluids **23**, 1336
[32]. Bornatici M et al, 1986, Plasma Physics and Controlled Fusion **28**, 629
[33]. Schkarofsky I, 1999, Journal of Plasma Physics **61**, 107
[34]. Karney C, 1986, Comp. Phys. Rep. **4**(3-4), 182
[35]. Lonnroth J, Parail V et al, 2004, Plasma Physics and Controlled Fusion **46**, 767
[36]. Suttrop W and Peeters A.G, 1997, IPP Report 1/306
[37]. Airoldi A and Ramponi G, 1993 , Proc. 20th EPS Conf. on Plasma Physics (Lisbon, Portugal), 6-39 p.III-1223
[38]. Wang Z et al, 1995, GA Report GA-A22038

Model	FP			MdM		
T_e	Δ	j_w	p_W, p_C	η, T_d[keV], v_d/c	j_d	p_{EE}
0.5keV	2	0.0031	2.16e-4, 2.48e-4	1.2e-3, 2keV, 0.1	0.0047	2.48e-4
	6	0.0044	2.49e-4, 2.80e-4	1.4e-3, 3.1keV, 0.11	0.0059	2.75e-4
1keV	2	0.0028	1.98e-4, 2.25e-4	1.1e-3, 4keV, 0.14	0.0032	2.32e-4
	6	0.0039	2.25e-4, 2.56e-4	1.3e-3, 6.1keV, 0.16	0.0043	2.52e-4
1.5keV	2	0.0026	1.86e-4, 2.14e-4	1.0e-3, 5.9keV, 0.18	0.0034	2.21e-4
	6	0.0036	2.11e-4, 2.40e-4	1.2e-3, 8.8keV, 0.19	0.0042	2.40e-4

Table 1: Results of MdM plateau fit to EDF by FP with $Z_{eff} = 1.5$, $E_{norm} = 0.002$, $D_0 = 0.05$, $w_1 = v_{ll}/v_{th} = 3.5$, $\Delta = 2$ and 6 and three bulk temperatures $T_e = 0.5$, 1 and 1.5keV. The cited current density values are normalised to e n vth while the power density to n m_e v_{th}^2 n_{te}. The driven current from FP, j_w, should ideally be equal to the MdM drift current j_d. The total absorbed LH wave power, p_W, and the collisional transfer to the bulk, p_C, derived from FP calculations and the collisional energy exchange rate, p_{EE}, between the bulk and the drift Mawellian part of MdM EDF are provided for comparison.

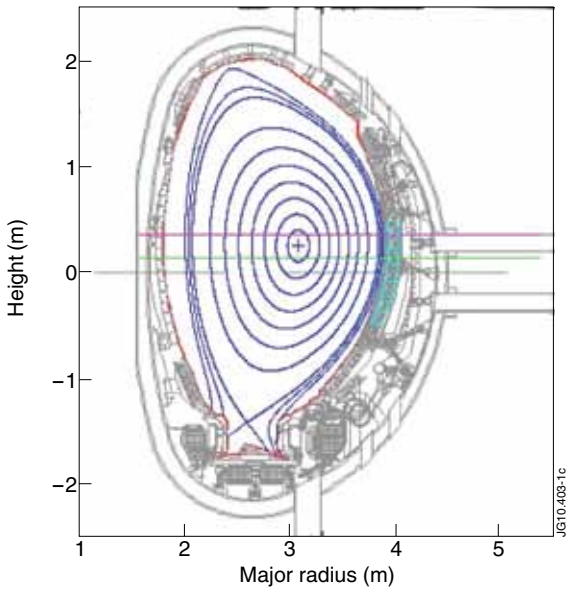

Figure 1: JET vessel, equilibrium flux surfaces (blue lines) for SS Pulse No: 72835, 7.00s, LOS of Michelson interferometer (magenta line) and radiometer (green line) and the position of the LH launcher (cyan line). All radial profiles shown in the study use the radius R_a, which is measured along the green line.

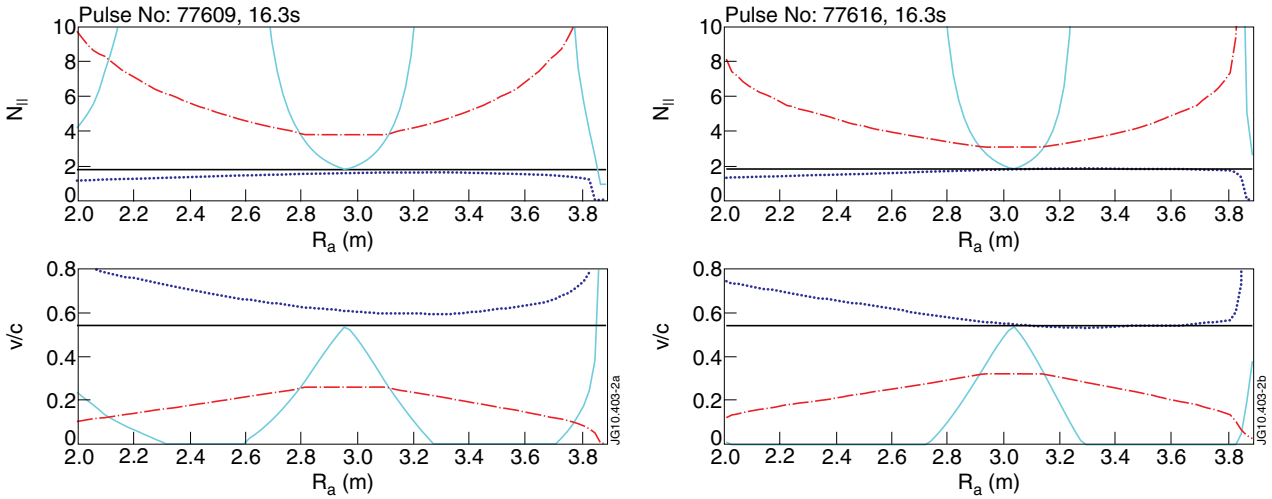

Figure 2. $N_{//}$ and v_{ph}/c versus R_a for 3.4T/1.8MA JET pulses at low Pulse No's: 77609 (a) and high density Pulse No: 77616 (b). The upper caustic $N_{//+}$ (solid cyan line) and the accessibility condition $N_{//acc}$ (dotted blue line) determine the wave propagation domain. The LH wave is launched with $N_{//}$ =1.84 (thin black line) and can propagate in the region $N_{//acc} < N_{//} < N_{//+}$. The wave will be significantly absorbed for values of $N_{//}$ approximately equal to $N_{//abs}$ (dashed-dotted red curve) corresponding to parallel velocities of the resonating electrons of about $3.5v_{te}$.

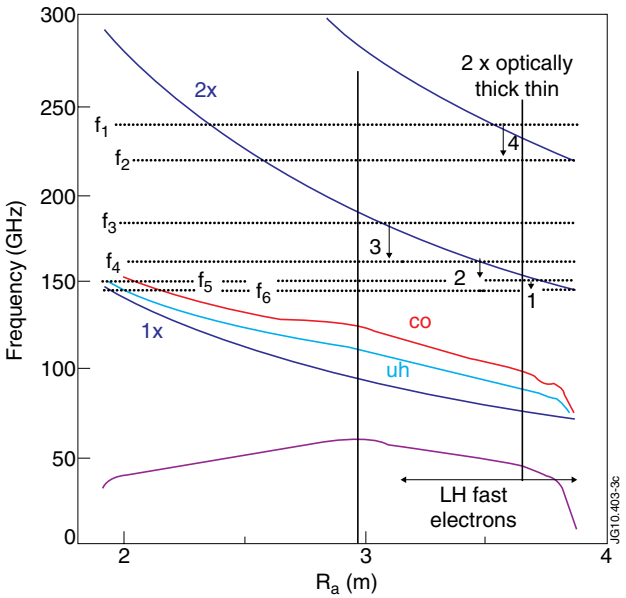

Figure 3: Radial dependencies of the 1st('1X' blue line), 2nd('2X' blue line) and 3rd (blue line) harmonic of the cyclotron resonance, cut-off ('co' red line) and upper hybrid ('uh' cyan line) frequencies for magnetic field of 3.4T. The LH fast electrons region is assumed between 3.10m and 3.86m and covers both the optically thin and the optically thick region in the plasma. EC downshifted emission in four particular cases of interest is given by vertical arrows numbered 1 to 4. Six relevant EC emission frequencies are noted by the symbols f_1 to f_6. Thermal electrons at about 3.13m will emit in 2X-mode at f_3 = 180GHz; however, fast electrons at that position with velocity $v/c \approx 0.44$ and relativistic factor of $\gamma_0 \approx 1.11$ will emit at downshifted frequency of $f_4 = f_3/\gamma_0 \approx 162$GHz and could possibly affect the measurements at 3.49m as shown by arrow 3. For slower electrons, e.g. $v/c \approx 0.26$ and $\gamma_0 \approx 1.04$, the downshift will be smaller, f_5 = 151GHz and $f_6 = f_5/\gamma_0 \approx 145$GHz as shown by arrow 1.

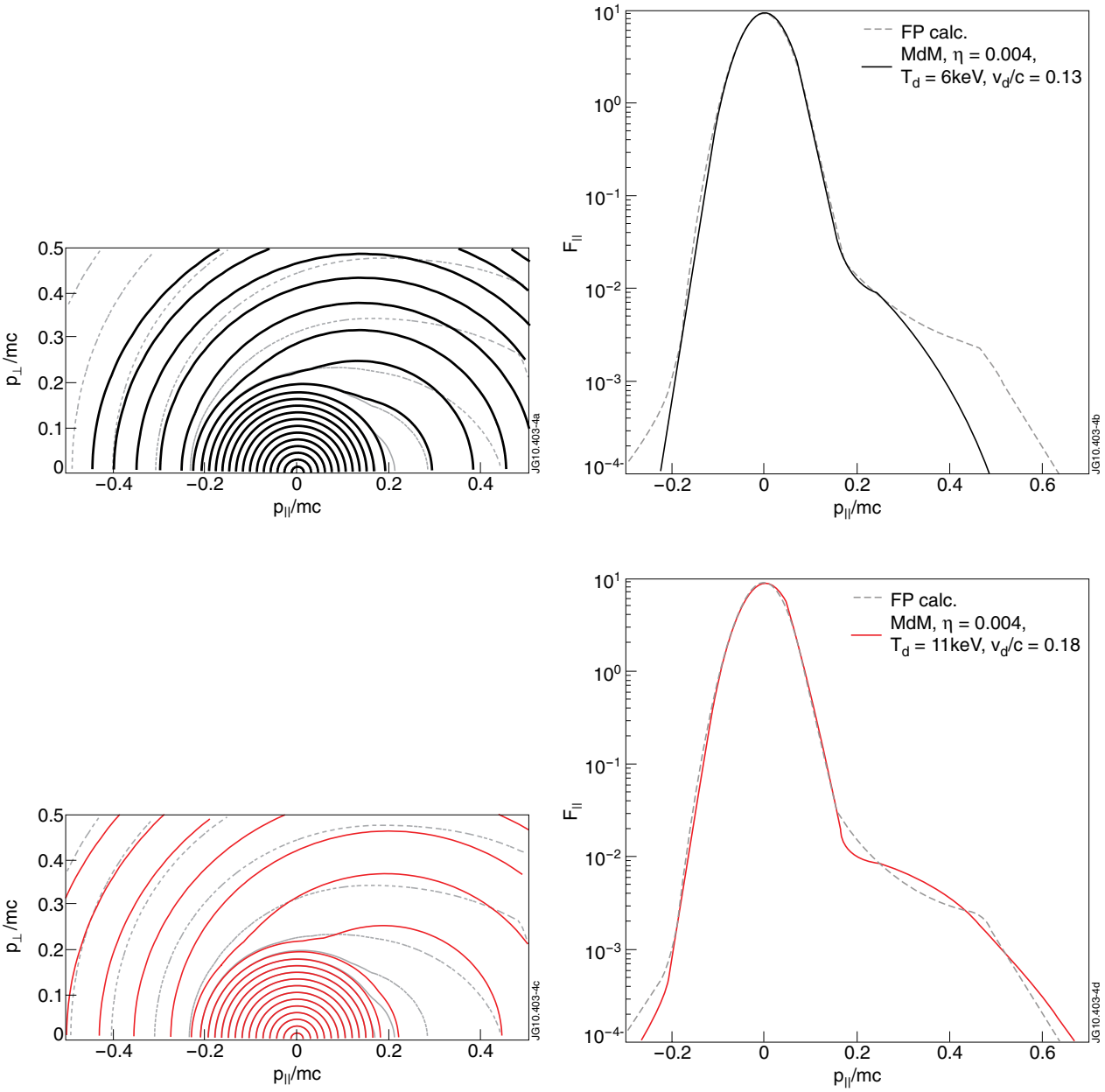

Figure 4: Contour plots of $f(p_\perp, p_{//})$ (a and c) and profiles of $F_{//}(p_{//})$ (b and d) from FP calculation with $Z_{eff} = 1.5$, T_e=1keV, $E_{norm} = 0.002$, $w_1 = v_{//}/v_{th} = 3.5$ ($v_{//}/c \approx 0.15$), $\Delta = 6$ and $D_0 = 0.1$ (dashed grey lines) and the corresponding fitted MdM EDF (solid black and red lines). The direct fit results given in black lines in a) and b) fail to reproduce the whole plateau. The fit to the FP plateau only displayed by red lines in c) and d) provides more reasonable estimate of the plateau with $\eta = 0.004$, $T_d = 11$keV and $v_d/c = 0.18$. The isolines in a) and c) are selected so that to give equally spaced contours with step $\delta p/mc \approx 0.015$ for a relativistic Maxwellian with T_e=1keV.

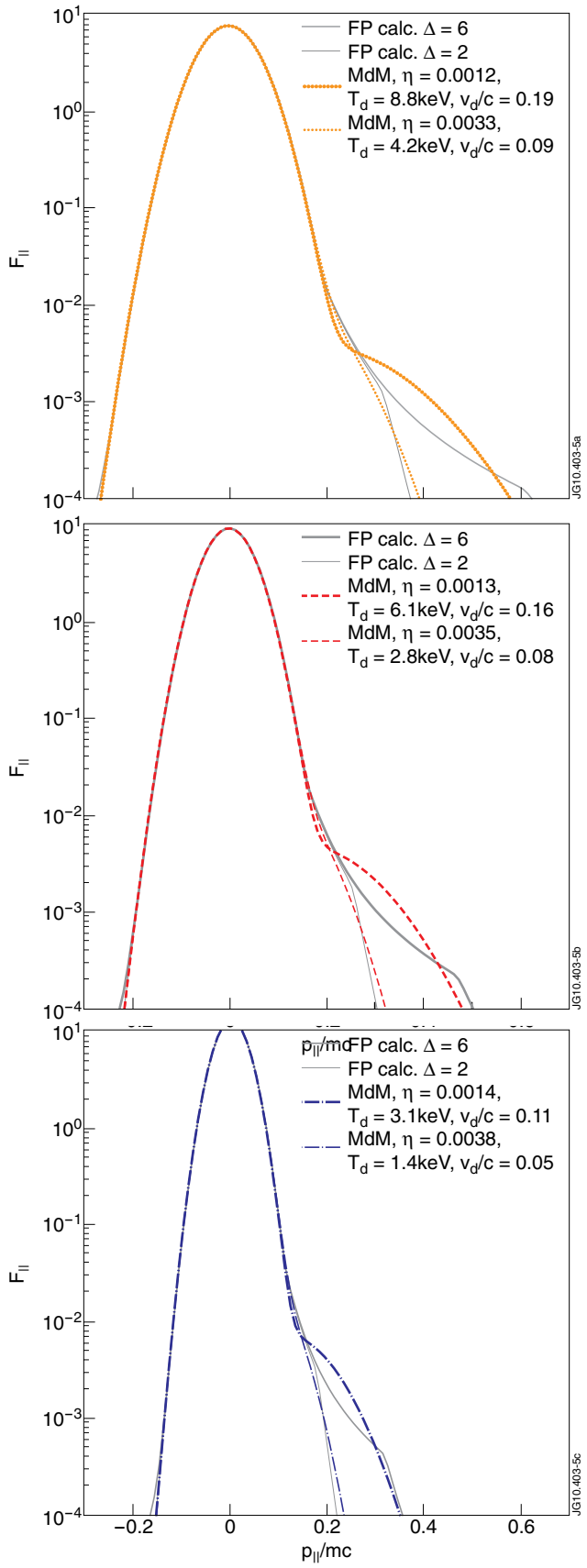

Figure 5: EDF $F_{ll}(p_{ll})$ from FP calculation (grey lines) with Z_{eff} = 1.5, E_{norm}=0.002, D_0 = 0.05, $w_1 = v_{ll}/v_{th}$=3.5, Δ = 6 (thick grey line) and Δ = 2 (thin grey lines) and three bulk temperatures T_e = 1.5keV(a), 1keV(b) and 0.5keV(c). The MdM fits to FP results are given as dotted orange (a), dashed red (b) and dash-dotted blue (c) lines as the corresponding MdM parameters are given in the figures' legends.

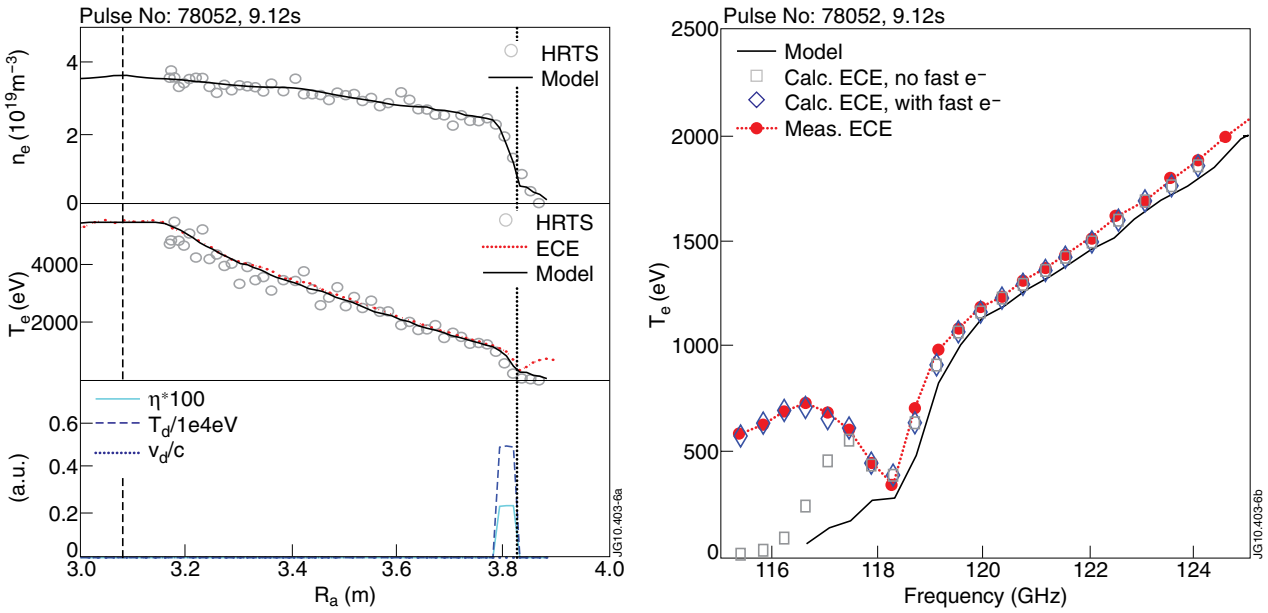

FIgure 6: EC emission in H-mode SS JET Pulse No: 78052, 9.12s at 2.7T/1.8MA plasma. Density and temperature profiles from HRTS (grey circles), ECE measurements (red dots) and the profiles used in the model (black curves) are shown together with the separatrix (dotted line) and magnetic axis (dashed line) in the top two graphs of (a). The drift Maxwellian parameters are shown in the bottom graph of (a). The results of the modelling are shown in (b) as plots of the ECE profiles versus frequency. The emission from Maxwellian plasma (grey squares) deviates from the measurements (red dots), while the emission in case of small fraction of fast electrons (blue diamonds) with $\eta \approx 0.0023$ (solid cyan line in (a)), $T_d \approx 5$keV (dashed blue line in (a)) and $v_d/c \approx 0$ (dotted blue line in (a)) matches better the experimental results. The frequency range in (b) covers the edge region from about 3.63m to about 3.9m.

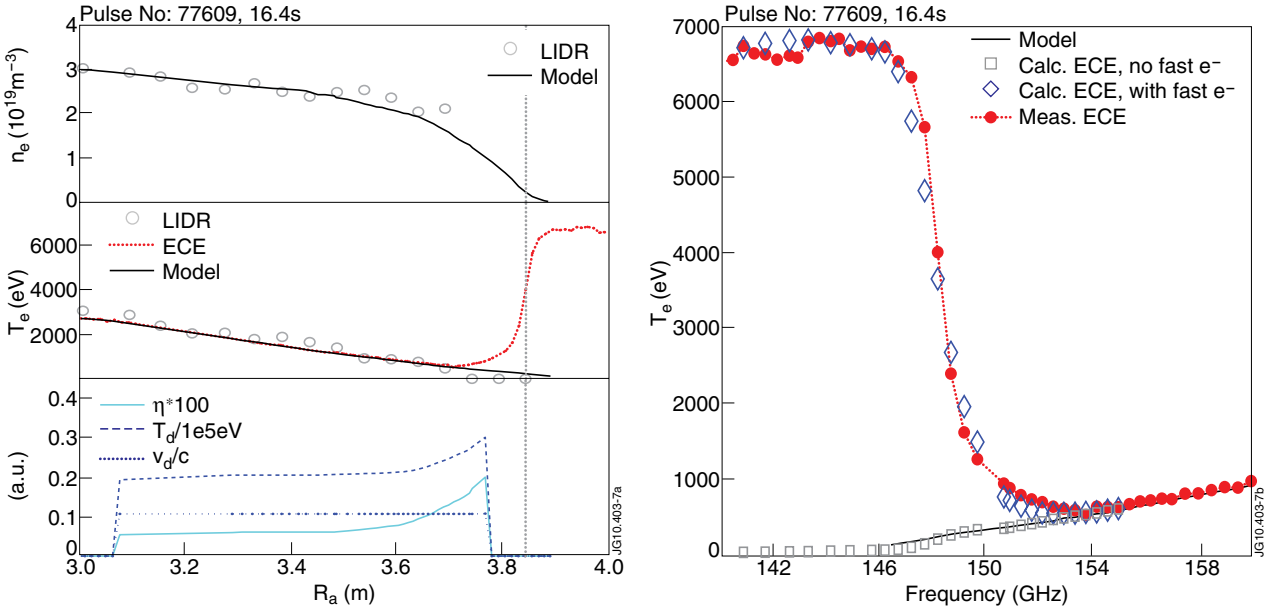

Figure 7. Electron density, n_e, temperature, T_e, and fast electron parameters η, T_d and v_d/c are shown in (a) for low-density L-mode 3.4T/1.5MA JET Pulse No: 77609, 16.4s. The grey circles on top two graphs in (a) indicate LIDAR measured profiles, while the black lines show profiles used in the model and separatrix is shown by dotted line. MdM EDF with η profile shown by solid cyan line in (a), T_d profile indicated by dashed blue line in (a) and $v_d/c = 0.01$ given by dotted blue line in (a) in the region $3.07\text{m} < R_a < 3.77\text{m}$ provide good match to the experimental ECE data as shown in (b). The calculated emission profiles (blue diamond symbols in (b)) using MdM EDF with such parameters are compared to the measured ones (red dots in (b)) and to the temperature profile used in the model (solid black line in (b)). The calculated ECE spectra in absence of fast electrons (grey squares in (b)) are provided for comparison.

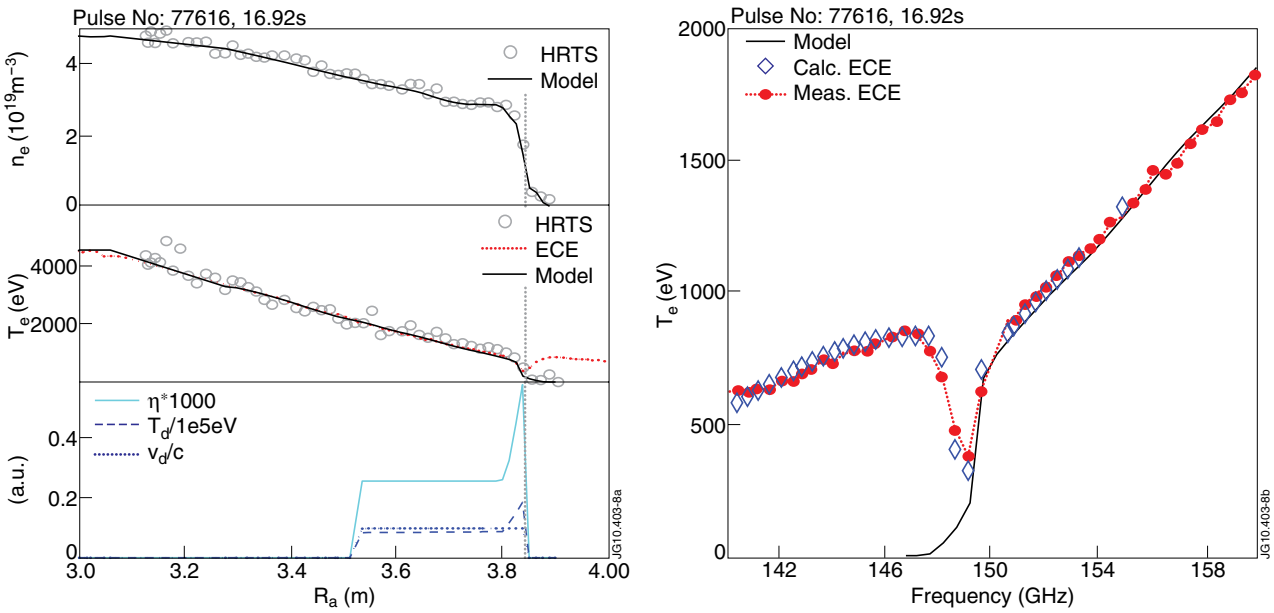

Figure 8. Electron density, n_e, temperature, T_e, and fast electron parameters η, T_d and v_d/c are shown in (a) for high-density H-mode 3.4T/1.5MA JET Pulse No: 77616, 16.92s. The grey circles on top two graphs in (a) indicate LIDAR measured profiles, while the black lines show profiles used in the model and separatrix is shown by dotted line. MdM EDF with η profile shown by solid cyan line in (a), T_d profile indicated by dashed blue line in (a) and $v_d/c = 0.01$ given by dotted blue line in (a) in the region $3.53m<R_a<3.84m$ provide good match to the experimental ECE data as shown in (b). The calculated emission profiles (blue diamond symbols in (b)) using MdM EDF with such parameters are compared to the measured ones (red dots in (b)) and to the temperature profile used in the model (solid black line in (b)).

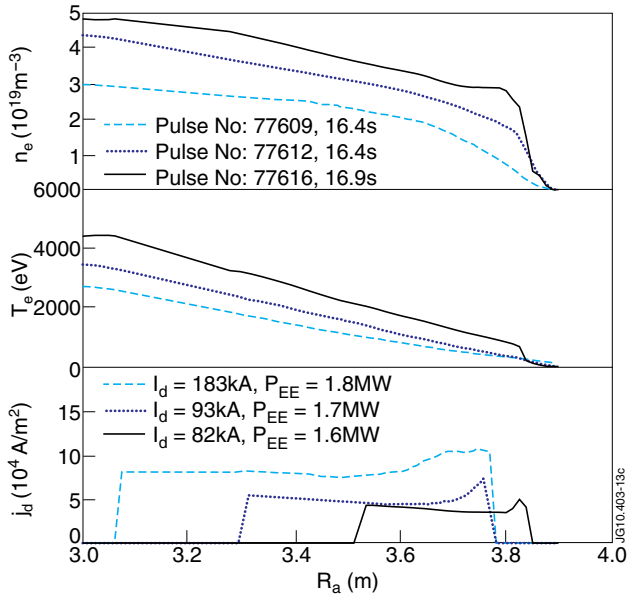

Figure 9: Electron density, n_e, temperature, T_e, and current density, j_{CD}, profiles for density scan pulses at 3.4T/1.5-1.8MA Pulse No's: 77609, 77612 and 77616.

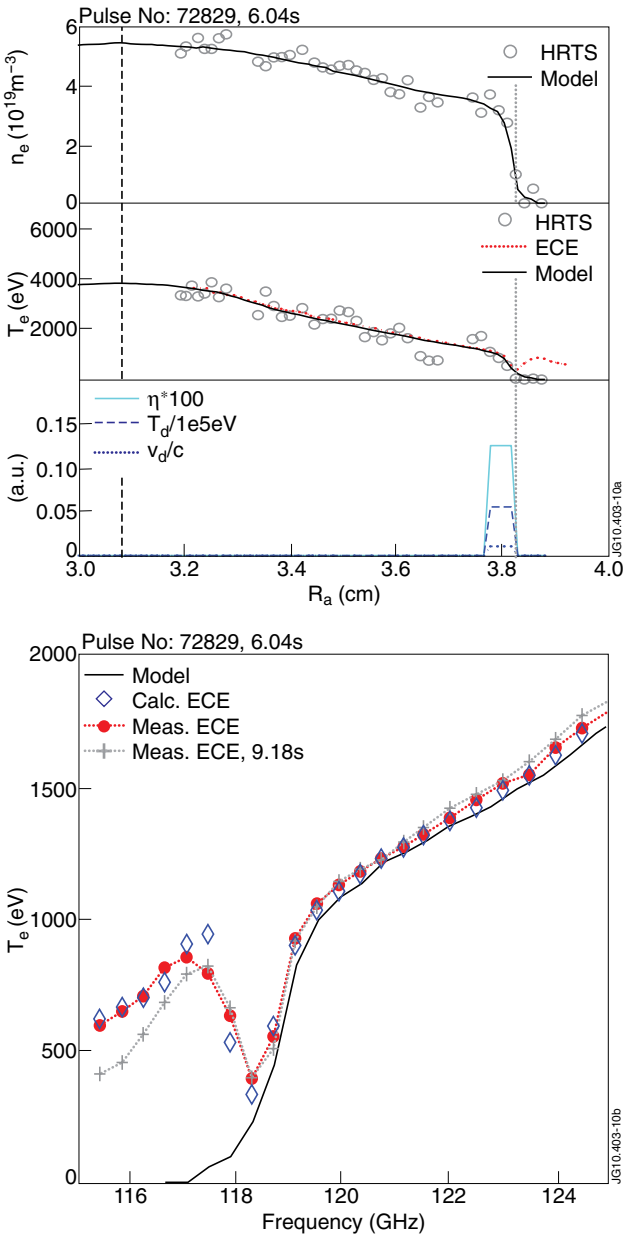

Figure 10: Electron density, n_e, temperature, T_e, and fast electron parameters η, T_d and v_d/c are shown in (a) for the high-density H-mode 2.7T/1.8MA JET Pulse No: 72829, 6.04s with P_{LH}=2MW. The grey circles on top two graphs in (a) indicate HRTS measured profiles, while the black lines show profiles used in the model and magnetic axis and separatrix are shown by dashed and dotted lines respectively. MdM EDF with η = 0.00125 (solid cyan line in (a)), T_d = 5.5keV (dashed blue line in (a)) and v_d/c = 0.01 (dotted blue line in (a)) in the region 3.78m<R_a<3.82m provide good match to the experimental ECE data as shown in (b). The calculated emission profiles (blue diamond symbols in (b)) using MdM EDF with such parameters are compared to the measured ones (red dots in (b)) and to the temperature profile used in the model (solid black line in (b)). The ECE spectra at 9.18s (grey + symbols in (b)) when the LH power was switched off, P_{LH} = 0MW, are provided for comparison.

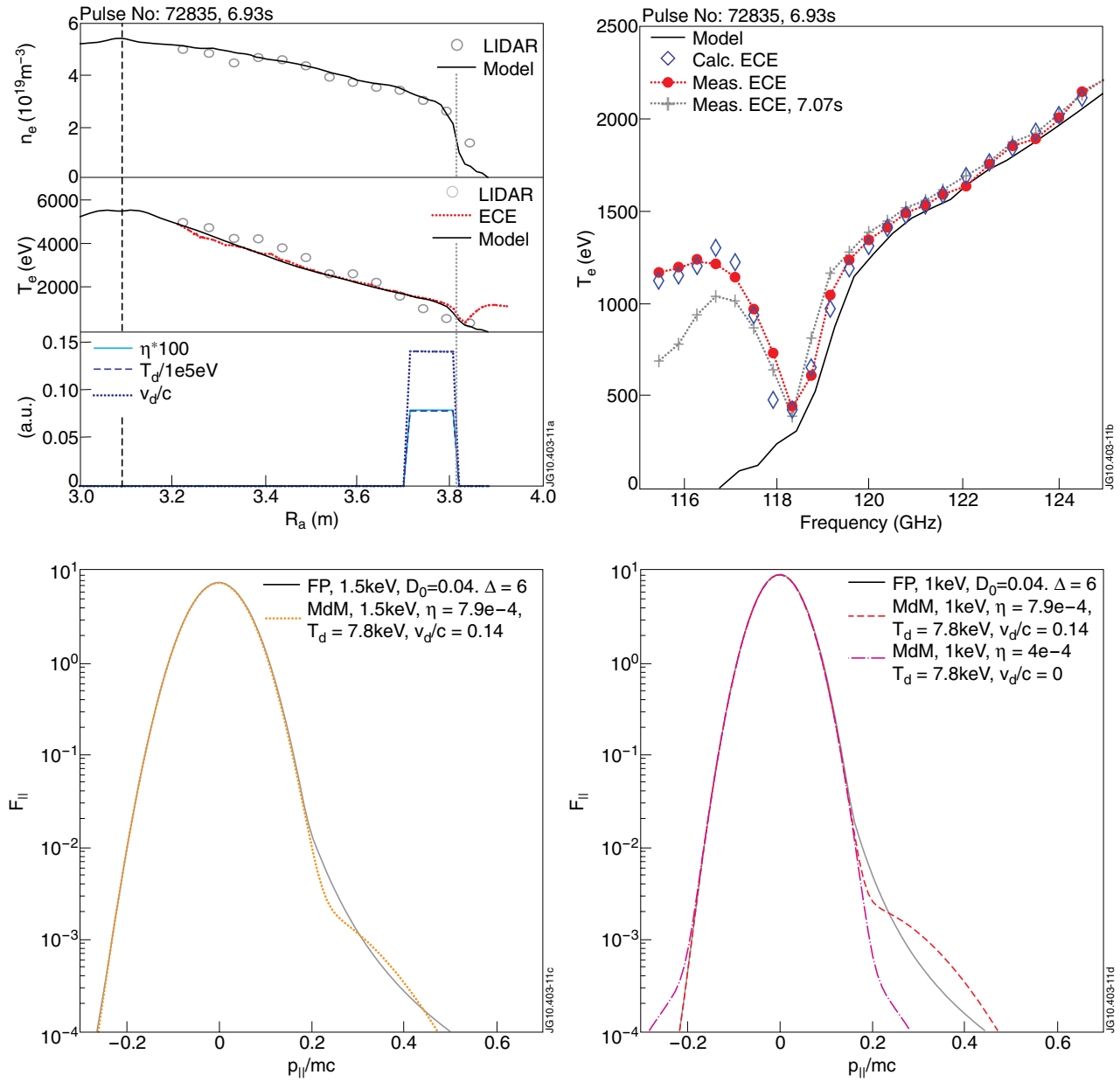

Figure 11. Profiles of electron density, n_e, temperature, T_e, and fast electron parameters η, T_d and v_d/c are shown in (a) for the high-density H-mode 2.7T/1.8MA JET Pulse No: 72835, 6.93s with P_{LH} = 2MW. On top two graphs the grey circles indicate LIDAR TS measured profiles, while the black lines show profiles used in the model and magnetic axis and separatrix are shown by dashed and dotted lines respectively. MdM EDF with η=0.00079 (solid cyan line in (a)), T_d = 7.8 keV (dashed blue line in (a)) and v_d/c = 0.14 (dotted blue line in (a)) in the region 3.72m<R_a<3.81m provide good match to the experimental data as shown in (b). The calculated emission profiles (blue diamond symbols in (b)) using MdM EDF with such parameters are compared to the measured ones (red dots in (b)) and the temperature profile used in the model (solid black line in (b)) is given as well. The ECE spectra at 7.07s (grey + symbols in (b)) when the LH power dropped to P_{LH} = 0.6MW are provided for comparison. The FP (solid grey lines) and MdM (dotted orange and dashed red lines) EDF are compared for 1.5keV (c) and 1keV (d) plasma. In (d) the MdM EDF (dash-dotted magenta line) needed to reproduce the EC emission in the non LH case is given for comparison.